Design and Optimization of Planar 3D Hall Effect Magnetic Position Sensors

Colin M. Pollard, Takara E. Truong, Tren Hirschi, and Mark A. Minor, *IEEE Member*

***Abstract*—A numerical approach to optimizing 3D hall-effect position sensors utilizing machine learning is proposed, estimating both sensing range, shape, and performance of the system. Optimization of design parameters are demonstrated with experimental validation, and overall design parameters of 3D magnetic position sensors are explored. Experimental results validate numerical simulations used for design. These principles are then applied to create a position sensor for a soft-robotics bladder for a Smart Helmet. Experimental validation of the resulting sensor configuration demonstrates ideal magnet size and tolerance for magnet misalignment.**

***Index Terms*—Hall Effect, Magnet Localization, Soft Robotics, Machine Learning**

I. Introduction

Traditionally, hall effect sensing has been used extensively for determining range of a magnet in one dimension. In recent years, position sensing in 3D has become more common for a variety of purposes. These sensors commonly consist of a large, grid shaped array of hall sensors on one or more planes, but can also be used in more compact, embedded solutions. These smaller sensors, modeled in Figure 1, consist of a distributed array of hall sensors on a compact circuit board, and determine the position of a planar magnet above the plane. Three-dimensional position can be obtained by using several sensor readings in combination with a variety of algorithms, such as machine learning. These sensors allow for position to be tracked using a passive embedded magnet, and simple electronics without the need for line-of-sight – something that for many soft-robotic applications is not possible.

While these sensors provide a great solution to non-line-of-sight position sensing, it is challenging to characterize the sensing region – the volume in which a magnet can be effectively tracked - and error of the system without experimental testing. Most designs of these sensors use a grid shaped hall sensor distribution and determine sensor parameters such as amplification and magnet choice based on what has worked experimentally. This research aims to provide a more precise method for predicting both factors of a given sensor using two simulation-based methods. The first algorithm characterizes fundamental types of error in these systems in 3D, allowing sensor design parameters such as amplification, and hall sensor patterning to be optimized for a desired sensing region. The second algorithm predicts a performance metric for the overall system configuration and allows parameters such as magnet choice to be optimized to minimize output error. Through these two methods, a sensor configuration can quickly be created that best fits a design specification for a specified sensing range, region, space, and error.

Finally, this research applies the simulation methods proposed to the design challenge of a smart helmet bladder and validates the results experimentally.

Paper submitted October 15, 2020. This work was supported by the US National Science Foundation under Grant #1622741.

C. Pollard, T. Hirschi, and M. Minor are with the University of Utah Department of Mechanical Engineering, Salt Lake City, UT. (e-mail: trenhir@gmail.com, colin.pollard1466@gmail.com, mark.minor@utah.edu).

T. Truong was with the University of Utah Department of Mechanical Engineering. He is now with Stanford University, Computer Science, Stanford, CA. (e-mail: takaraet@gmail.com).

II. Related Work

Hall effect sensors have been used in one dimensional position tracking extensively. In the simplest case, a hall-effect sensor can be used as a position switch, such as in keyboards, printers, and combustion engine timing. In more complex cases, they can be used for continuous position solutions such as in truck transmissions [1], and linear position estimation [2]. To that end, Honeywell created a guide for many of these use cases that outlines the basic design optimization of several configurations [3]. These configurations include “head on” and “slide-by” where the magnet is moving in the direction of the sensing element, and laterally to the sensing element respectively. In these modes, the math to resolve position from field strength is simple, consisting of an inverse tangent fit.

These 1D position sensing cases can be extended to 3D configurations through the addition of distributed hall sensors. This capability is valuable for a variety of uses, including

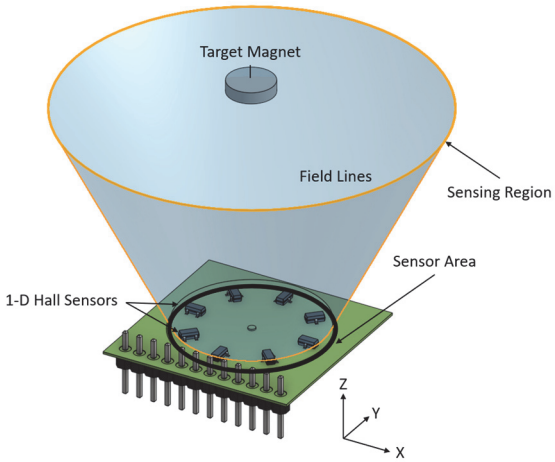

Figure 1 Basic Sensor Design.

gesture detection for wearable devices [4], and tracking of a stylus on a screen [5, 6]. Notably, these systems have been used widely in tracking of endoscopes through the GI tract [7] and in localization and characterization of soft robotic elements [8].

To resolve 3D position, several approaches have been explored. These include a Jacobian-based approach [9] that obtains a closed form solution based on finite-element analysis, a Levenberg-Marquardt algorithm approach [10], graph optimization [11], and pure dipole modeling [12]. While each of these approaches are proven to work well, artificial neural networks (ANNs) can be used to solve the same problem [13, 14] with more simplicity. While each of these approaches are proven to work well, artificial neural networks (ANNs) can be used to solve the same problem [12, 13] with more simplicity. ANNs can also use computational resources, which can make them an ideal choice for embedded systems. By utilizing a regression fit machine learning algorithm, the need for precise sensor mounting, magnet selection, and other factors are baked into the training data set that is unique to each sensor, and the error due to experimental variation can be reduced. Since this study is focused on optimization of the physical sensor design and not the algorithm, machine learning was chosen.

Optimization of 3D hall position sensors have been explored for GI endoscope tracking [14, 15]. It is found in [15] that multiple planes of sensors around the subject increases accuracy. This is further explored in [10] where the sensing area is surrounded by hall effect sensors. While these provide valuable insight into performance of multi-plane sensors, this paper seeks to find a method of position sensing using Hall effect sensors which can be applied in various applications that only allow a single sensing plane, such as the Smart Helmet and Smart Shoe [16, 17].

Localization and characterization specifically of soft robotic elements is a challenge with several current solutions, which are usually specific to the application. Some examples of such systems include using optical sensors and infrared sensors [18, 19]. However, when line of sight is not guaranteed, such as in [20, 21], the sensing requirements or obstacles require a different approach, where Hall effect sensors can excel. Applications in soft robotics that use Hall effect sensors include soft force sensors [22, 23].

The performance of different algorithms has been compared for planar sensors [24], but besides overall size of the sensor system [8], the physical design parameters of these systems have been mostly treated as a constant. This paper seeks to characterize the fundamental types of error present in planar 3D position hall sensors, and extrapolate sensor design parameters (such as amplification, magnet choice, etc.) from predicted error regions, and signal performance.

III. Sensing System

A. Hardware

The basic architecture of a 3D hall effect position sensor is shown in Figure 2. The system consists of four main parts: an array of 1-D hall effect sensors, an amplification stage, an analog to digital conversion, and finally a machine learning algorithm.

For the purposes of this exploration, the Hall Effect array consists of Texas Instruments DRV5055 sensors distributed within a single plane. The amplification layer used in this exercise is based around the TLV2734 amplifier. A differential configuration with an offset of 1.65V removes negative field solutions.

Due to the planar orientation of the sensors and known magnet orientation, we can assume that any negative field strength is an invalid result. Because of this, the amplification stage removes the offset voltage and scales the remaining voltage as shown in (1).

$$V_{out} = Gain * \left(V_{in} - V_{offset}\right)$$
$$V_{out} = Gain * \left(V_{sensor} - V_Q\right)$$
$$V_{out} = Gain * Sensitivity * \left|\vec{B}\right| \quad (1)$$

After amplification, amplified signals are routed into a Teensy 4.1 which handles analog to digital conversion, data logging of the sensor voltages to portable storage, and processing through the machine learning algorithm. These values can then be logged, used for system control algorithms - such as helmet bladder pressure control, or exported through a communication bus.

B. Machine Learning Algorithm

This study employs an empirically selected 3-layer feedforward neural network, 1 input layer, 1 hidden layer, and 1 output layer. The input layer consists of 10 nodes representing hall effect voltage signals. The hidden layer includes 20 nodes. The output layer consists of 3 nodes that yields position (x,y,z). This configuration is less computationally intensive and is should be well suited to operate on a micro controller in future work. Levenberg-Marquardt was used to train the neural network model.

IV. Characterizing Configuration Induced Errors

For a 3D position to be resolved with single-dimension magnitudes, such as those from hall effect sensors, there must

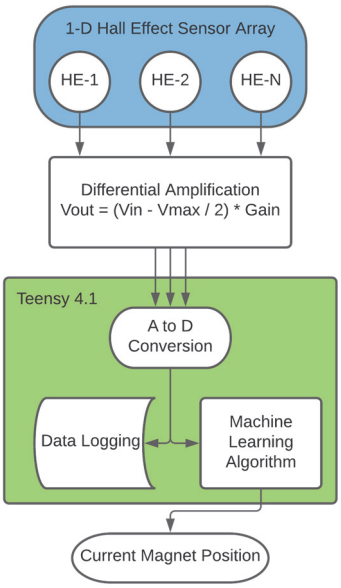

Figure 2. Sensor Architecture Diagram.

be at least four valid sources of this information. This process is referred to as trilateration and is well described by Wolfram's online demonstration [25]. In the case of a planar sensor where the sensing space is mechanically bound to above the plane, only three readings are required. Similarly, the differential amplification technique will electrically constrain the solution space to be above the sensor plane.

For analog hall effect sensors, there are two ways in which a reading is invalid. A sensor can "**saturate**" if there is too strong of a magnetic field at the sensor's position, and the output voltage will clip. A sensor can have too weak of a magnetic field available and produce a voltage small enough that it falls below the noise floor of the system, referred to as **"floored"**. These two effects can be visualized in Figure 3, where the voltage of various sensitivity sensors is plotted as a function of magnet distance. While these types of readings technically do provide information to the system (the field is strong enough to saturate or weak enough to floor) they will be treated as invalid for the purposes of this characterization.

A. Error Characterization Algorithm

The input to the Error Region Characterization Algorithm consists of a full system configuration. These include a magnet source, hall array pattern, and voltage function that describes the sensitivity and amplification. The output of the algorithm is a set of 3D points, each with a status flag. The status flag can be one of three states – valid point, saturated point, floored point. These points can then be plotted and analyzed. From this information, the area in which the sensor can theoretically resolve a solution is revealed, and the reason for error is characterized.

The algorithm breaks the problem down as shown in Figure 4. This process starts by iterating through every point in the Raster Space. This space consists of uniformly distributed points inside a cube above the sensor plane. At each point, a status flag is generated based on the sum of the individual hall effect sensor readings. If at least three sensor readings are determined to be valid, the point status is set to valid. If there are not three valid readings, the point is determined to be invalid and the flag is set to the majority error cause.

For each sensor at a point, the magnetic field strength in 3D is calculated using magpylib [26]. The Z-axis portion of the magnetic field is utilized as the field strength parameter in (1) and the sensor voltage is estimated. If the sensor voltage is above the supply voltage, clipping has occurred and the sensor is saturated. If the sensor voltage is near zero (within a small offset such as 5mV), the sensor is floored. Otherwise it is valid.

After each hall effect sensor produces a result, the data is aggregated into a point result, and then these point results are aggregated into a total solution space. These solution spaces are plotted in 3D using a colored scatter chart, Figure 6.

B. Magnetic Field Exploration

As an example, a 3X3 array of DRV5055 sensors is simulated with a cylindrical magnet. These sensors are equally arrayed within a one-inch square and use a differential amplifier with various gain settings. Using the Error Characterization Algorithm, we can see how various magnetic field properties can manifest as error in our sensing system.

1) Magnetic Field Strength

The strength of the sensing magnet can greatly affect the error of the system. A strong magnet increases the minimum sensing distance, while a weak magnet reduces the maximum sensing distance. These effects can be viewed as regions of saturation and flooring. To visualize this effect, a narrow column directly above the sensor plane is selected over a long z-distance. Figure 5 was generated using a 3x3 grid sensor pattern, spanning 30mm. Each sensor is modeled after a DRV5055-A1 amplified with 10V/V gain. From this figure, there is a clear sensing floor shown in purple. This region represents saturation error where the sensor voltage is clipping at the maximum voltage. At the top of the space there is the sensing ceiling shown in blue. This is a region of flooring,

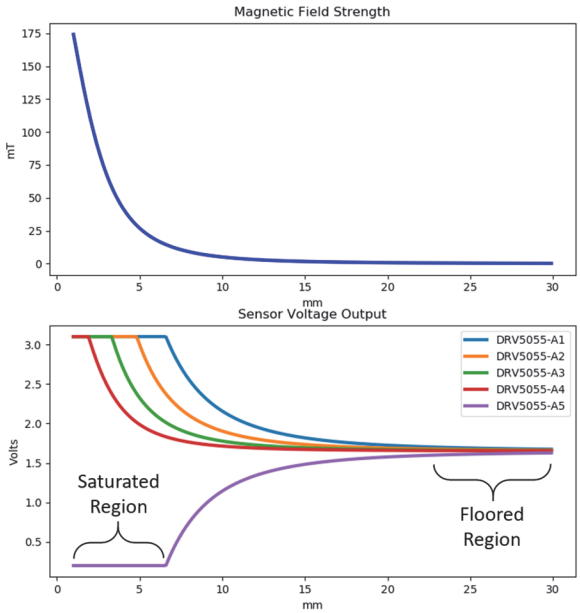

Figure 3. Hall Sensor Voltage Sweep

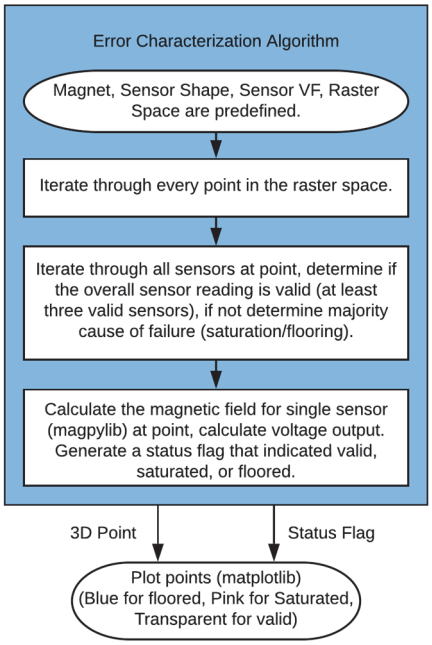

Figure 4. Error Characterization Algorithm Block Diagram.

where the sensors do not have produce sufficient voltage to make a valid reading. This threshold is set at 3.2mV, matching that of a 3.3V ADC with 10-bit resolution. The saturation region appears to span from 0-9mm above the sensing plane, and the flooring region is around 320mm above the plane. Based on these types of results, the amplification and magnet can be chosen to best fit the desired range.

2) Magnetic Field Geometry

Characterizing error in this manner is also useful for optimizing the field shape. Since these sensors are based on 1-D hall effect sensors, as the field direction shifts from vertical directly under the magnet towards horizontal the readable voltage changes drastically. This is what allows these sensors to decern 3D position, but also puts a limit on the sensing range in the planar direction. By utilizing 3D error plots, horizontal range can be characterized just as vertical range was previously.

Figure 6 was generated using the same magnet and sensor configuration as in Figure 5, truncated for all $X < 0$, and only includes the highest error point in each X, Y column. This is done to create a clearer picture of the 3D shape. This demonstrates a square bowl shape error region (blue) where the field geometry no longer affects the sensors in a meaningful way. To illustrate this point further, a flow chart of the magnetic field lines is generated in the Y=0 plane at a magnet position inside the valid region, and outside the valid region.

In Figure 7 there are two points shown. The first is created where the magnet is in a valid point. The second point is outside of this region and was characterized as a floored point. As shown by the field lines, the first point is valid because the orientation of the magnetic fields that intersect the sensors (in red) is primarily in the vertical Z direction – in phase with the 1D hall effect sensors. The second point demonstrates that as the magnet travels further in the X-direction, the field lines become more horizontal (out of phase with the hall effect sensors) and at an extreme, reverse polarity.

By utilizing this algorithm, the process of drawing magnetic field line charts for each point are abstracted away into a general classification.

C. *Application – Truncation of Training Data*

One of the core challenges of using machine learning to fit regression problems is selecting valid data input. As shown previously the magnetic field geometry can very rapidly convert from valid data to error. This problem can be countered by using simulation to truncate training data. Training data from 4 trials using different magnets were truncated. The output error of the validation sets are shown in Table 1.

For trials 1, 2, and 3, truncating the data lowered mean error. However, in trial 4, the error increased. This is because for the first three trials, the training raster occupies a significantly larger space than the valid sensing region. For trial 4, the sensing space is close in size to the valid range. As the number of invalid points in the training space increases, the error reduction from truncation will increase, however when the spaces are matched, the algorithm can remove questionable data that the machine learning algorithm can use to fit the model.

Table 1. Output Error

Trial	1	2	3	4
No Manipulation Error (mm)	15.76	5.53	4.6	9.99
Raster Truncation Error (mm)	15.09	5.27	4.36	10.59

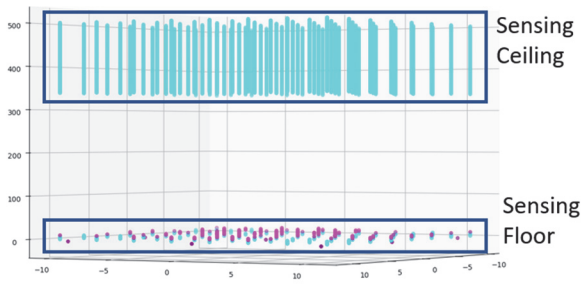

Figure 5. Error Characterization Plot of Sensing Ceiling and Floor.

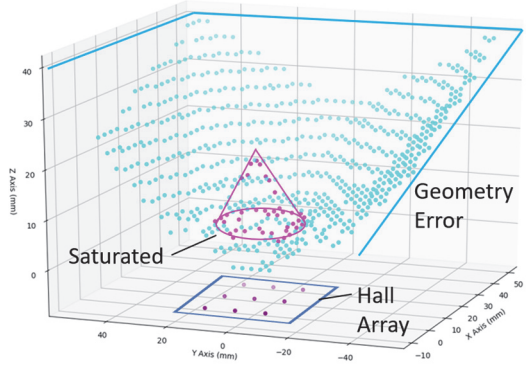

Figure 6. Error Characterization of Field Geometry Error.

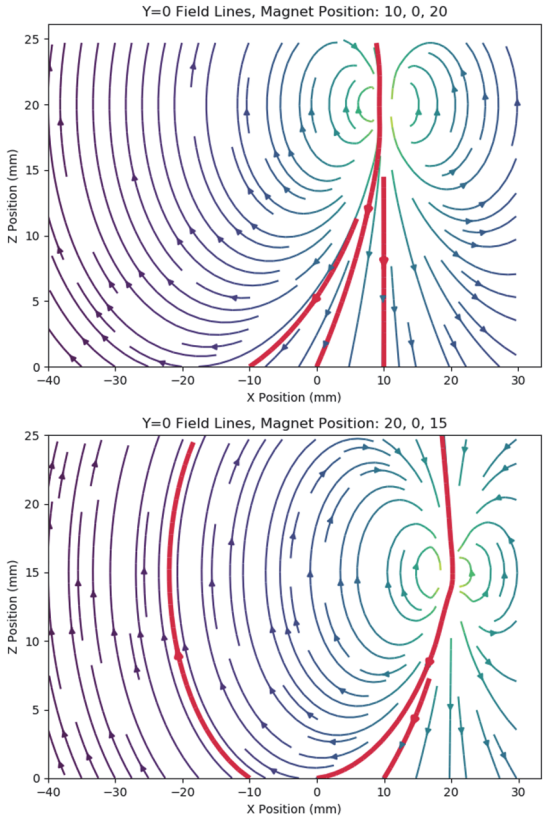

Figure 7. Field Lines for Valid and Invalid Positions

D. Validation

1) Experimental Setup

A Teensy4.1 MCU was connected to three stepper motor drivers, moving the x, y, and z axis of a modified 3D printer. The printer has an assembly installed in place of the extruder where magnet cartridges can be interchanged. The sensor under test is placed in a rigid holder (jig) shown in Figure 8 and remains stationary while the magnet cartridge moves above the plane. Sensor data is collected through the Teensy, and data is exported to an SD card for processing in MATLAB and python.

2) Results

To validate the error characterization algorithm, raster scans were run on the test equipment described above with identical sensor and magnet configurations to simulations. The raster scan voltage values are then characterized by the algorithm alongside an identical simulation. The output values are differenced and the error is shown in Table 2.

The validation for the error characterization algorithm shows a pessimistic view of the raster data. While it perfectly characterizes the invalid points in the raster data, it also classifies additional valid data as invalid. This is because the simulation uses perfect functions to model the system, such as planar sensor and magnet mounting. For instance, if each hall effect sensor is rotated in a different direction to the plane, there are more opportunities to sense heavily curved fields. As shown earlier, the primary cause of flooring error is field geometry that is too sharp to sense with a planar sensor, so a random mounting could result in more valid points. Additionally, the maximum field strength that could be experienced is when the magnet is parallel to the sensors. In the real world the maximum strength is most likely never experienced due to mechanical tolerance and as such the simulation predicts more saturation. To validate this, reducing the simulation magnet's strength reduces the saturation false positive rate (to 6%) without affecting the false negative, while flooring error remains the same due to geometry – implying maximum field strength is never experienced.

V. Optimizing Sensor Error

While error characterization is an effective method for determining root causes of error and optimizing sensing shapes, it does not provide a metric of the overall system performance. To accomplish an overall estimate, we utilized a gradient simulation. Regression fitting problems benefit from higher signal to noise. In this case, more change in voltage for a change in position should yield better performance from the machine learning algorithm. The block diagram of this algorithm is shown in Figure 9.

The algorithm moves through a series of points in a raster space, and at each point it determines the validity using the error algorithm. After a point is determined to be valid, the gradient is estimated by moving the magnet by a small delta position in each direction. The square of the voltage change of each direction is then summed and recorded. This can be displayed as either a 3D plot of best performance regions or aggregated into an overall configuration score. With this single score, a series of gradient simulations can be run with a changing parameter, and where the maximum gradient is predicted, the lowest error should be observed. This algorithm is applied and validated in the case study.

VI. Analysis of Results

A. Magnetic Field Geometry

As explored previously, one of the most fundamental restrictions of these sensors is the error due to magnetic field geometry. For a given sensor configuration, there is a critical distance where the field lines are no longer sensible. This is most notable around the edges of hall sensor arrays at close Z distances. When designing a new sensor, if mechanical constraints permit, the sensing array should extend laterally past the desired sensing region to limit this effect. Additionally, the density of hall effect sensors should be high enough such that these edge effects are not experienced while inside the array. To determine this density, an error characterization simulation can be created and if no floored points are observed above the plane, the density is adequate such as in Figure 10.

Table 2. Sensing Error Validation

Error Type	Total Error	False Positive	False Negative
Saturation	13.61%	13.61%	0%
Flooring	25.27%	25.27%	0%

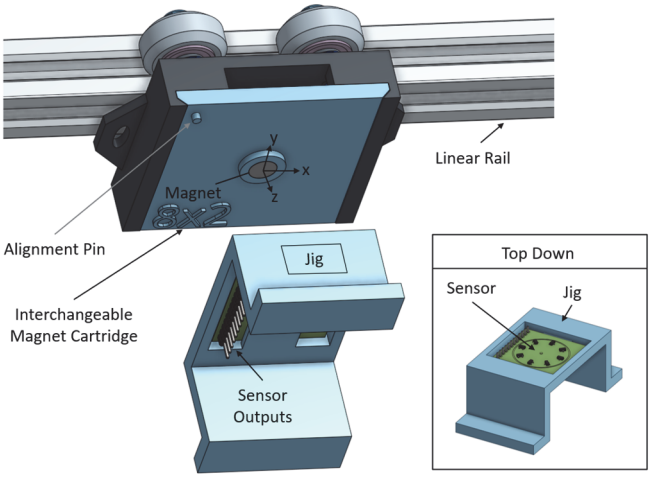

Figure 8. Raster Test Bench

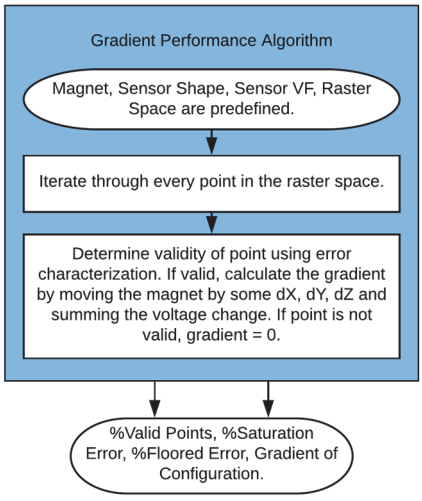

Figure 9. Gradient Block Diagram.

B. Sensor Shape

Depending on application needs, the shape of the sensing region can be tailored by changing the pattern of the hall-effect array. Intuition into a given sensor shape can be gathered using an error algorithm simulation.

For large scale arrays, the patterning is not as important provided that the sensor density is high enough to not leave gaps in the sensing space. In compact sensors, the edge effect explained in part A is less avoidable. For a given sensor pattern, there is a region around the edge that is still sensible before field geometry renders the solution invalid. This allows for specific edge shapes to be created to best fit a problem. For instance, circular patterning can create a conical edge case while square grids can create a prismatic edge case. While in general the shape of the sensing region follows the outline of the hall patterning, density of sensors will affect the exact shape.

C. Number of Sensors

Using a gradient simulation, the number of sensors in a space can be varied to provide better region coverage and performance. Figure 11 highlights the effect of different numbers of hall sensors distributed along the perimeter of a 1" circle. Performance is analyzed in a 40mm^3 space. From the bottom error plot, at small sensor quantities, the majority of the region cannot be resolved (only around 10%). Additionally, from the first plot, the gradient of the system does increase with sensor quantity throughout the sweep, while error sees diminishing returns after around 10 sensors.

D. Magnet Strength

Magnet strength as a design parameter is not as clear cut as it first seems. Based on the 1D design guides published by Honeywell [3], they suggest choosing the highest sensitivity sensor that does not saturate. In general, a higher strength magnet will increase the fundamental signal (magnetic field strength), and therefore create a higher signal to noise ratio. This can create problems with amplification however, as magnet strength combined with amplification will determine the minimum and maximum sensable distance. For sensors that need long distance sensing regions, a high strength magnet combined with high amplification will allow for the best performance at long distance at the expense of minimum sensing distance. Conversely, a lower strength magnet may create a more balanced profile for medium and short range applications.

E. Amplification

Amplification is related to magnet strength, and independent of magnetic field geometry. This is demonstrated in Figure 10, where amplification is compared from 1X, 2X, 5X, and 10X respectively. The inner purple saturation region increases in size as the amplification increases, while the floored blue region remains mostly the same due to field geometry. As amplification grows, the number of invalid saturated points also grows, but the points that are valid will have a higher gradient. Depending on application, increasing amplification could create a higher performing region, or a longer range sensor at the expense of minimum sensing distance.

VII. Case Study – Smart Helmet Bladder Sensing

A. Smart Helmet Background

The Smart Helmet project aims to reduce traumatic brain injury (TBI) through active control of impact absorption [17]. By utilizing instrumented soft-robotic bladders instead of traditional absorption material, the helmet aims to detect the location and strength of an impact. Control algorithms can to open or close valves that interconnect the bladder array and disperse the impact. These bladders require compact embedded electronics that can sense deformation through the position of the top of the bladder and pressure.

B. Design Constraints

The design of a bladder Figure 13 (left), consists of a compressible chamber molded on top of a base. Bladders are mounted on the interior of the helmet shell, Figure 13 (right), and incorporate sensing and valving to control impact forces. The base of each bladder contains ports for air, as well as the embedded electronics. The base must be thin such that the compressible distance is maximized, limiting the position sensing technology significantly. Several sensing technologies were tested for this application, including IR range finding, and

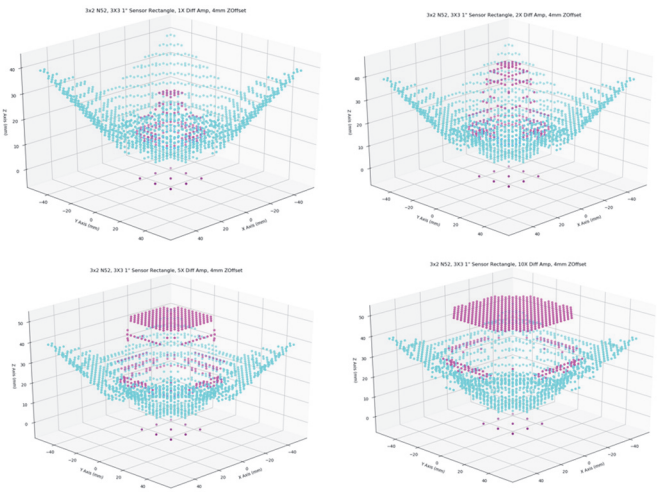

Figure 10. Amplification Comparison.

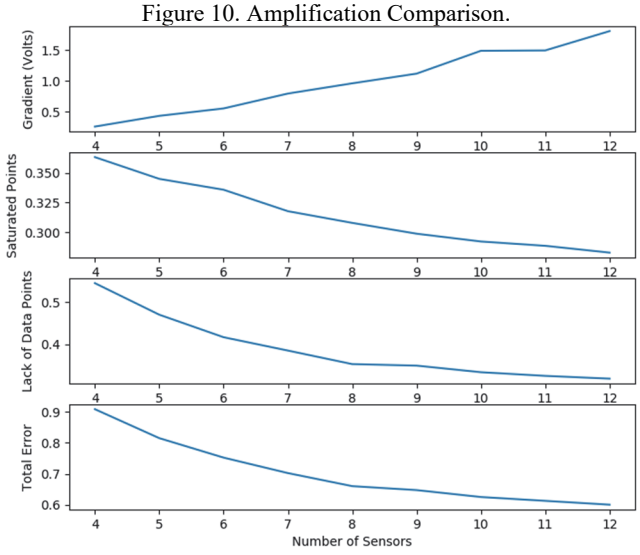

Figure 11. Effect of number of sensors.

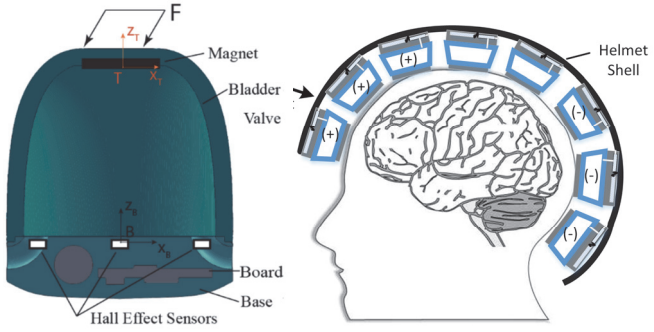

Figure 13. Smart Helmet bladder (left) and helmet diagram illustrating bladder placement (right).

ultrasonic range finding. While IR sensors do exist at this compact size, the silicon material proved difficult to measure at distances past 20mm above the sensor and silicon walls occasionally obstructed the sensor. Ultrasonic sensors were not compact enough. Hall effect sensing proved to be an effective solution, as it could localize 3D position instead of just 1D, and fit in the mechanically allowed area.

The current generation bladder is up to 40mm tall, and based on previous testing, can deform laterally to around half of its height. This creates an ideal sensing region that is 40X40X40mm. Additionally, the hall-effect array cannot extend outside of the bladder base, forcing a pattern that has a diameter less than 30mm. Using these two restrictions, simulation can be used to optimize other sensor parameters.

C. *Design Process*

The first challenge is designing a sensor pattern that will maximize coverage inside the desired sensing region. The hall effect array is constrained inside of a circle, and the sensing region is cylindrical – ideal for a circular pattern of hall effect sensors. The error characterization algorithm was then used to determine how large the sensor pattern needed to be. Based on these results, the array did not need to be the full diameter of the bladder base. A diameter of 1 inch was chosen to allow for trace routing room around the sensors, while maintaining adequate region coverage. Based on the pre-existing 10 channel analog to digital converter, 10 hall effect positions were created equally arrayed around the circumference.

With the sensor array configuration and size established based on 3D error simulations, two parameters remain to be optimized – magnet choice and amplification. Amplification was chosen to be 10 V/V gain to obtain a balance of accuracy and range, determined by both gradient and error simulations. Magnet choice is partially limited by the allowable thickness of the bladder walls to 2mm, but the diameter can be optimized using a gradient simulation, Figure 12. From this simulation, the ideal diameter magnet would be 2mm, with a second maximum at 8mm.

D. *Performance Analysis*

Five commercially available N52 magnets were used to gather training and test sets using the experimental setup described in IV D. The performance of each type of magnet is assessed in Table 3. From these results, there is a clear inverse relationship between the mean error and the predicted gradient. This is expected as a higher signal to noise should yield a lower error. This validates that the simulation successfully optimized the magnet diameter for this configuration.

E. *Effect of angled magnet*

Table 3. Performance based on Magnet Diameter.

Up to this point the magnet has been assumed to be parallel with the hall array plane. However, in most applications this is not a valid assumption. For instance, in the Smart Helmet bladder, there is a possibility for the magnet to be rotated by small angles, which could increase position error. To evaluate the sensitivity to angle sensitivity, three different magnet cartridges were created each holding a magnet at an angle in the x-z plane. The sensor configuration from the helmet case study was used, and three identical 8mm magnets were tested. As seen in Table 4, at small angles, magnet tilt has a small impact on error, which is acceptable in most applications. However, in areas where magnet tilt could exceed small angles, desensitization [13] or 5D sensing would be more applicable.

VIII. Conclusion

Through this exploration, we have provided several tools for assisting with the evaluation of 3D hall effect position sensors. The first tool, error characterization, can predict the region a given sensor can operate in using simulation. The results from

Magnet Diameter (mm)	Mean Test Set Error (mm)	Predicted Gradient
3	11.13	12.08
5	5.27	11.17
8	4.36	14.32
12	10.59	10.03

Table 4. Effect of Magnet Angle

Magnet Tilt (degrees)	Mean Error (mm)	Error to Control (%)
0	4.59	0
5	4.647	+1%
10	4.828	+5%

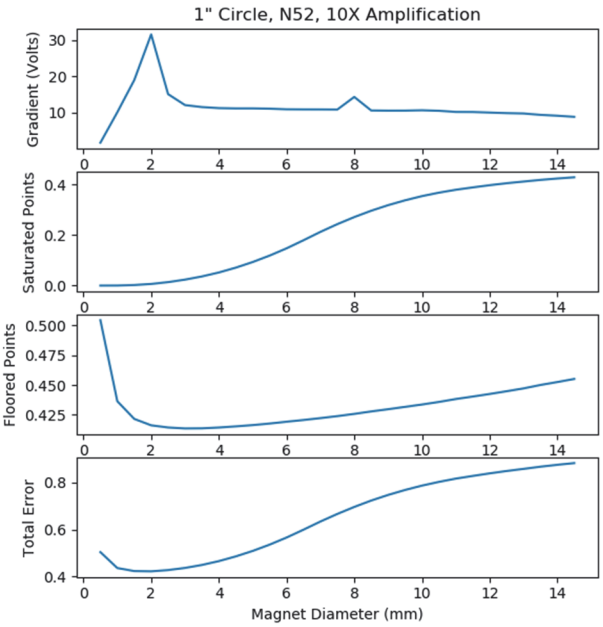

Figure 12. Circle Sensor Diameter Optimization

this can be used to evaluate the range of a sensor, the volume it can resolve position in, and help inform design decisions such as hall sensor patterning based on the amount, shape, and type of error observed.

The second tool, gradient simulation, allows for relative error performance to be predicted for a given sensor configuration. Most importantly, a series of gradient simulations can be created where a sensor design parameter is changing. From the predicted gradient, the ideal permutation can quickly be selected, creating a better performing sensor.

These two methods were then applied to optimize the design of a smart helmet bladder sensor. This first used error characterization to create a sensor pattern that best fit the deformation of a bladder, and then gradient simulation to choose the best magnet size for minimal error.

IX. Future Work

As noted in the error characterization algorithm validation, precise angular mounting of sensors has a great effect on the severity of error due to magnetic field geometry. In future works, a factor could be added to this simulation method that approximates the effect of imperfect mounting to improve error estimation.

Another important metric, slew rate / update rate, was not touched on in this exploration. In the future, it would be valuable to train several sensors and use a fast, closed-loop control test bench to measure error as a function of velocity.

Lastly, in an application like the smart helmet, several position sensors would be used in close proximity – creating a chance for interference between sensors. Possible mitigation strategies include combining the hall effect data from all of the arrays into one regression fit problem that localizes several positions at a time, effectively converting the other magnet sources from noise into data sources, or utilizing more complex fields that are less likely to interfere with each other.

References

[1] J. O. Manyala, T. Fritz, and M. Z. Atashbar, "Integration of Triaxial Hall-Effect Sensor Technology for Gear Position Sensing in Commercial Vehicle Transmissions," *IEEE Transactions on Instrumentation and Measurement,* vol. 61, pp. 664-672, 2012.

[2] J. Kim, S. Choi, K. Cho, and K. Nam, "Position Estimation Using Linear Hall Sensors for Permanent Magnet Linear Motor Systems," *IEEE Transactions on Industrial Electronics,* vol. 63, pp. 7644-7652, 2016.

[3] (10/11/2020). *HALL EFFECT SENSING AND APPLICATION*. Available: https://sensing.honeywell.com/hallbook.pdf

[4] K.-Y. Chen, K. Lyons, S. White, and S. Patel, "uTrack: 3D input using two magnetic sensors," in *Proceedings of the 26th annual ACM symposium on User interface software and technology*, St. Andrews, Scotland, United Kingdom, 2013, pp. 237–244. 10.1145/2501988.2502035.

[5] R.-H. Liang, K.-Y. Cheng, C.-H. Su, C.-T. Weng, B.-Y. Chen, and D.-N. Yang, "GaussSense: attachable stylus sensing using magnetic sensor grid," in *Proceedings of the 25th annual ACM symposium on User interface software and technology*, Cambridge, Massachusetts, USA, 2012, pp. 319–326. 10.1145/2380116.2380157.

[6] P. Berkelman and H. Abdul-Ghani, "Electromagnetic Haptic Feedback System for Use With a Graphical Display Using Flat Coils and Sensor Array," *IEEE Robotics and Automation Letters,* vol. 5, pp. 1618-1625, 2020.

[7] D. Son, S. Yim, and M. Sitti, "A 5-D Localization Method for a Magnetically Manipulated Untethered Robot Using a 2-D Array of Hall-Effect Sensors," *IEEE/ASME Transactions on Mechatronics,* vol. 21, pp. 708-716, 2016.

[8] C. D. Natali, M. Beccani, N. Simaan, and P. Valdastri, "Jacobian-Based Iterative Method for Magnetic Localization in Robotic Capsule Endoscopy," *IEEE Transactions on Robotics,* vol. 32, pp. 327-338, 2016.

[9] S. Song, C. Hu, and M. Q. Meng, "Multiple Objects Positioning and Identification Method Based on Magnetic Localization System," *IEEE Transactions on Magnetics,* vol. 52, pp. 1-4, 2016.

[10] S. Su, H. Dai, S. Cheng, P. Lin, C. Hu, and B. Lv, "A Robust Magnetic Tracking Approach Based on Graph Optimization," *IEEE Transactions on Instrumentation and Measurement,* vol. 69, pp. 7933-7940, 2020.

[11] Y. Ren, C. Hu, S. Xiang, and Z. Feng, "Magnetic dipole model in the near-field," in *2015 IEEE International Conference on Information and Automation*, 2015, pp. 1085-1089. 10.1109/ICInfA.2015.7279448

[12] F. Wu, N. M. Robert, D. D. Frey, and S. Foong, "Enhanced magnetic localization with artificial neural network field models," in *2013 IEEE International Conference on Robotics and Automation*, 2013, pp. 1560-1565. 10.1109/ICRA.2013.6630778

[13] N. Sebkhi*, et al.*, "A Deep Neural Network-Based Permanent Magnet Localization for Tongue Tracking," *IEEE Sensors Journal,* vol. 19, pp. 9324-9331, 2019.

[14] C. Hu, T. Ma, and M. Q. Meng, "Sensor Arrangement Optimization of Magnetic Localization and Orientation system," in *2007 IEEE International Conference on Integration Technology*, 2007, pp. 311-315. 10.1109/ICITECHNOLOGY.2007.4290485

[15] K. M. Popek, T. Schmid, and J. J. Abbott, "Six-Degree-of-Freedom Localization of an Untethered Magnetic Capsule Using a Single Rotating Magnetic Dipole," *IEEE Robotics and Automation Letters,* vol. 2, pp. 305-312, 2017.

[16] Y. Wang and M. A. Minor, "Design and Evaluation of a Soft Robotic Smart Shoe for Haptic Terrain Rendering," *IEEE/ASME Transactions on Mechatronics,* vol. 23, pp. 2974-2979, 2018.

[17] J. P. Aston*, et al.*, "Optimization of a Soft Robotic Bladder Array for Dissipating High Impact Loads: an Initial Study in Designing a Smart Helmet," in *2020 3rd IEEE International Conference on Soft Robotics (RoboSoft)*, 2020, pp. 607-614. 10.1109/RoboSoft48309.2020.9116034

[18] T. C. Searle, K. Althoefer, L. Seneviratne, and H. Liu, "An optical curvature sensor for flexible manipulators," in *2013 IEEE International Conference on Robotics and Automation*, 2013, pp. 4415-4420. 10.1109/ICRA.2013.6631203

[19] H. Thien, M. Stommel, F. L. Daheron, A. L. Page, Z. Deng, and W. L. Xu, "Embedded infrared imaging to measure the deformation of a soft robotic actuator," in *2016 International Conference on Image and Vision Computing New Zealand (IVCNZ)*, 2016, pp. 1-6. 10.1109/IVCNZ.2016.7804428

[20] J. Jung, M. Park, D. Kim, and Y. Park, "Optically Sensorized Elastomer Air Chamber for Proprioceptive Sensing of Soft Pneumatic Actuators," *IEEE Robotics and Automation Letters,* vol. 5, pp. 2333-2340, 2020.

[21] Y. Yang and Y. Chen, "Innovative Design of Embedded Pressure and Position Sensors for Soft Actuators," *IEEE Robotics and Automation Letters,* vol. 3, pp. 656-663, 2018.

[22] S. Youssefian, N. Rahbar, and E. Torres-Jara, "Contact Behavior of Soft Spherical Tactile Sensors," *IEEE Sensors Journal,* vol. 14, pp. 1435-1442, 2014.

[23] T. P. Tomo*, et al.*, "A modular, distributed, soft, 3-axis sensor system for robot hands," in *2016 IEEE-RAS 16th International Conference on Humanoid Robots (Humanoids)*, 2016, pp. 454-460. 10.1109/HUMANOIDS.2016.7803315

[24] G. D. Angelis, A. D. Angelis, A. Moschitta, and P. Carbone, "Comparison of Measurement Models for 3D Magnetic Localization and Tracking " *Sensors,* vol. 17, 2017.

[25] (10/15/2020). *Trilateration and the Intersection of Three Spheres* [Demonstration]. Available: https://www.wolframcloud.com/objects/demonstrations/TrilaterationAndTheIntersectionOfThreeSpheres-source.nb#:~:text=Trilateration%20is%20used%20in%20technologies,space%2C%20such%20as%20orbiting%20satellites.

[26] (2019). *magpylib* [Python Library]. Available: https://github.com/magpylib/magpylib